Preprint typeset using LaTeX style emulateapj v. 01/23/15

1 Draft version May 4, 2017

RECONSTRUCTING THE EVOLUTIONARY HISTORY OF GRS 1915+105

Charles Kimball[1]

Draft version May 4, 2017

ABSTRACT

We present a hybrid methodology for reconstructing the evolutionary histories of low-mass x-ray binaries given observational constraints. We apply this methodology to GRS 1915+105 and present probability densities for system parameters at birth, the moments just before and just after the core-collapse and supernova of GRS 1915+105's black hole progenitor, and at the onset of roche-lobe overflow. We find that GRS 1915+105's black hole progenitor entered the main sequence with a mass between either 6.9-8.0, 28.0-30.8, or 41.6-42.4 $M_{\odot}$, before shedding its envelope in a common envelope phase and undergoing core-collapse between either 6.3-7.6, 12-12.4, or 17.7-18.1 $M_{\odot}$, resulting in a black hole between 5.6 and 12.7 $M_{\odot}$. We also use proper motion data to trace the trajectory of GRS 1915+105 through the galactic potential, using ages from our stellar models to predict probable birth sites, and find that the system center-of-mass received a kick between 11.7 and 157.2 km/s during supernova.

1. INTRODUCTION AND OBSERVED PROPERTIES OF GRS 1915+105

Transient black-hole x-ray binaries (BHXRBs) are composed of a stellar-mass black hole (BH) accreting from a companion star that is overfilling its Roche lobe. If the companion is less massive than the BH, its orbit will widen as mass as transferred through the L1 Lagrange point toward the accretor. The increasing wealth of data on the galactic population of BHXRBs makes them an excellent probe of compact object formation. However, that sort of insight requires that we piece together their histories back through multiple distinct stages of evolution, which is a task of tall order.

In their 2005 paper, Willems at al. applied a patch-work technique to take advantage of relatively new mass estimates and proper motion data to reconstruct the evolutionary history of the BHXRB J1655-40, providing insight into the birth of its black hole accretor and evidence that the system received a natal kick during the core-collapse of the BH progenitor. This study seeks to apply the general methodology of Willems et al. (2005) to the BHXRB GRS 1915+105 and eventually all BHXRBs with proper motion data, taking advantage of the availability of increasingly precise measurements and modern, state-of-the-art stellar evolution software. Following the analysis of a similar study by Sørensen et al. (2017), we will use the results of a massive population synthesis simulation to weight and constrain the properties of GRS 1915+105 at each stage of its evolution: The birth of its BH progenitor, the moments just before and after supernova, and at the onset of Roche-lobe overflow (RLO). Below we outline the observational properties of GRS 1915+105 before outlining our general approach.

GRS 1915+105 is a very wide BHXRB with a period of 33.85 $\pm$ 0.16 days (Steeghs et al. 2013). Its black hole accretor is the heaviest among transient BHXRBs with a recent measurement by Reid et al. (2014) putting it at 12.4 +/- $2M_{\odot}$, and has an extremely high spin of $a^* = a/\mathcal{M} \geq 0.98$ (McClintock et al. 2006). Its donor companion is a K-III giant with a relatively low mass of 0.58 +/- 0.38 $M_{\odot}$, derived from Steegh et al.'s 2013 estimate of a mass ratio of $M_{DON}/M_{BH} = 0.042$ +/-0.024. Proper motion data given by Miller-Jones (2014) puts its peculiar velocity at a relatively low 36 +/-22 km/s. For a more complete overview of the observed properties of GRS 1915+105, see Table 1 below.

2. OUTLINE OF METHODOLOGY

2.1. *Motivation*

Suppose we consider model Θ^j of a possible progenitor system at some evolutionary stage k with parameters θ_k^j. Further, suppose that during its mass transfer phase, the model has observables X_j when it satisfies the observational constraint on its period[1] We seek the posterior probability $p(\theta_k^j|X_{obs})$ that GRS 1915+105 did indeed have parameters θ_k^j given its current observables X_{obs}. We apply Bayes' Theorem and write:

$$p(\theta_k^j|X_{obs}) = \frac{p(X_{obs}|\theta_k^j)p(\theta_k^j)}{p(X_{obs})} \quad (1)$$

[1] This project, unfinished but slowly wrapping up, is the consequence of work and input by many people. In addition to the guidance of my advisor Dr. Vicky Kalogera, her graduate student Niharika Sravan, collaborator Dr. Tassos Fragos, and his graduate student Mads Sørensen (both at the University of Geneva), this project is built on the work of undergraduate student Slobodan Mentovic and masters student Aprajita Hajela. Although I will be writing the paper for this study, I do not present this as a rough draft of our work nor list everyone as authors because they have not had the chance to approve what I have written here and my mistakes should not reflect on them. This is a write-up of our work to date for the partial fulfillment of my honors degree here at Northwestern.

[1] The orbital period of GRS 1915+105 is by far the strictest constraint, so it is useful to think of taking a "snapshot" of a model when P_{orb}=$P_{orb,obs}$ for comparison to the observational constraints.

TABLE 1
Observed Properties of GRS 1915+105

Parameter	Notation	Value	σ +/(−)	Reference
Orbital Period ($days$)	$P_{orb,obs}$	33.85	0.16	1
Black Hole Mass ($M_\odot$)	$M_{BH,obs}$	12.4	2.0(1.8)[a]	2
Donor Mass ($M_\odot$)	$M_{DON,obs}$	0.58[b]	0.33	1,2
Mass Ratio	q_{obs}	0.042	0.024	1
Donor Effective Temperature ($Kelvin$)	$T_{eff,obs}$	4100-5433[c]		3,4
Black Hole Spin Parameter	$a_{*,obs}$	$\geq$0.98[d]		5
Distance (kpc)	d	11.0	1.0	1,6,7
Galactic Longitude (°)	l	45.37		1,6,7
Galactic Latitude (°)	b	-0.22		1,6,7
U (km/s)[e]	U	272	23	1,6,7
V (km/s)[e]	V	-230	23	1,6,7
W (km/s)[e]	W	11.0	4	1,6,7

References. — [1] Steeghs et al (2013); [2] Reid et al (2014); [3] Fragos et al (2015); [4] Gray D.F. (2008); [5] McClintock et al (2006);[6] Miller-Jones (2014) [7] Dhawan et al (2007)

[a] In the case of asymmetric error bars, we take the larger value as one sigma

[b] Derived using the value of q from Steeghs et al (2013) and the more recent value of M_{BH} from Reed et al (2014)

[c] This is not a direct measurement with associated uncertainties. Rather, it is a range of possible values of T_{eff} derived from reported spectral types. We adopt the range used by Fragos et al (2015), derived from tables in Gray D.F. (2008)

[d] This is a lower limit reported by McClintock et al (2006) based on spectral analysis.

[e] U , V, and W are the velocity components of GRS 1915 with respect to our local standard of rest (LSR). Positive values point along $l = 0°$, $l = 90°$, and $b = 90°$ respectively. All spacial and kinematic data is taken from tables compiled in Miller-Jones (2014) and derived from Steeghs et al (2013) and Dhawan et al (2007)

As in Sørensen et al. (2017), we assume that the errors in Table 1 are Gaussian, and evaluate the likelihood

$$p(X_{obs}|\theta_k^j) = \mathcal{L}(\theta_k^j|X_{obs}) = \prod_i \mathcal{G}(x_i^j;\mu_i,\sigma_i), \qquad x_i^j \in X_j, \quad (\mu_i,\sigma_i) \in X_{obs} \tag{2}$$

where

$$\mathcal{G}(x;\mu,\sigma) = \frac{1}{\sqrt{2\pi\sigma^2}} e^{\frac{-(x-\mu)^2}{2\sigma^2}} \tag{3}$$

is the normal distribution.

Meanwhile, our prior probability has

$$p(\theta_k^j) \propto n(\theta_k^j) \tag{4}$$

where n is the number density of systems with parameters θ_j^k at evolutionary stage k in the galactic population. Since we are interested in the relative probability of a given possible progenitor system (PPS) being the "true" progenitor over another PPS, this proportionality is good enough. We neglect $p(X_{obs})$ for the same reason.

2.2. *Obtaining $p(\theta_k^j)$ and $p(X_{obs}|\theta_k^j)$*

As in Willems et al. (2005), we limit our investigation to the "standard" evolutionary channel for LMXRBs. Namely, we assume that GRS 1915+105 began as a binary with a massive primary that loses most of its hydrogen-rich envelope in a Common Envelope phase, leaving a helium star and a lower-mass and hence less-evolved companion. Possibly receiving a kick upon the helium star's core-collapse and black hole formation, the binary then evolves until the companion fills its roche lobe, at which point mass transfer begins. Since no single technique can account for this entire evolution in a computationally feasible way, we break it into four stages and address them separately, investigating the parameter-spaces at the moments bookending each stage: The very beginning of the binary's life, when the primary and companion begin hydrogen burning and enter the main sequence; The moments just before and after core collapse; and at the onset of mass-transfer, when the companion first fills its roche lobe. The corresponding parameter spaces are θ_{ZAMS}:($M_{1,ZAMS}$, $M_{2,ZAMS}$, A_{ZAMS}, e_{ZAMS}); θ_{preSN}:($M_{BH,preSN}$, $M_{DON,preSN}$, A_{preSN}, e_{preSN},V_k); θ_{postSN}:($M_{BH,postSN}$, $M_{DON,postSN}$, A_{postSN}, e_{postSN}); and θ_{RLO}:($M_{BH,RLO}$, $M_{DON,RLO}$, $P_{orb,RLO}$). This study is a combination of the methodologies seen in Willems et al. (2005) and Sørensen et al. (2017). Namely, we take the treatment of systems from pre-supernova to RLO from the former, and the treatment of systems from ZAMS to pre-supernova from the latter. We begin with the last stage, using MESA (Modules for Experiments in Stellar Astrophysics, see Paxton et al. (2015) for the latest instrument paper), a state-of-the-art 1-D stellar evolution code, to evolve a grid of combinations of $M_{BH,RLO}$,$M_{DON,RLO}$,$P_{orb,RLO}$, each representing a PPS at RLO, onwards through the mass transfer phase. We then evaluate whether, at any point in its evolution, the PPS simultaneously

satisfies the observational constraints on the period, black hole mass, mass ratio, and effective temperature listed in Table 1. Each system that satisfies the constraints gets marked as a "winner", and its observables[2] are used to evaluate the terms on the right-hand side of equation 2. By tying every PPS from each stage of our reconstruction to exactly one of these winning mass transfer sequences, this gives us one approximation of $p(\theta_k^j|X_{obs})$ that covers every stage k.

Besides the observables listed above, we include an additional term in equation 2. Using the spatial and kinematic data for GRS 1915+105 compiled in Miller-Jones (2014), we integrate its trajectory backwards in time through the galactic potential and record its peculiar velocity each time it crosses the galactic plane. Identifying the galactic disk as the most likely birth location of the black hole progenitor, this gives us a distribution of possible peculiar velocities upon being kicked out of the disk during supernova. We then compare the peculiar velocities obtained by our supernova calculations to this distribution to assign a weight that functions as a term in equation 2.

With $p(X_{obs}|\theta_k^j)$ taken care of, we then focus on our prior, $p(\theta_k^j)$. Starting with a flat[3] distribution of ZAMS parameters, we use a publicly available parametric binary stellar evolution code known as BSE (see Hurley et al. (2013)) to evolve a large population of stellar binaries until core-collapse. For each system that has survived this evolution, we sample one thousand kick velocities, kick directions, and remnant masses, and use conservation of energy and angular momentum considerations to obtain post supernova orbital parameters.

Since detailed tidal evolution calculations involving the stellar structure of the companion are computationally expensive, it would be unfeasible to evolve all of our post supernova systems forwards towards RLO. Instead, we draw pairs of $M_{BH,RLO}$, $M_{DON,RLO}$from our winning mass transfer sequences to use as post supernova masses[4], and take a grid of post supernova orbital separations and eccentricities for each of them to integrate orbital parameters until the onset of RLO. Since each pair of $M_{BH,RLO}$ $M_{DON,RLO}$can correspond to multiple winning mass transfer sequences, we calculate each systems angular momentum to match it to a unique triplet ($M_{BH,RLO}$, $M_{DON,RLO}$, $P_{orb,RLO}$) and hence a unique MT sequence. Finally, we compare the post-supernova properties from our BSE and SN calculations to identify systems that fall within a cell of the grid of post supernova properties used for the tidal evolution. By way of the tidal sequences, each PPS is tied together from ZAMS all the way through RLO. The multiplicity of systems with a given set of parameters then furnishes our prior $p(\theta_k^j)$.

3. MASS TRANSFER PHASE

We begin by constraining the parameter space at the onset of RLO using a semi-analytic approach. Namely, we seek to identify potential progenitors at the onset of RLO (PPRLO), with properties $M_{BH,RLO}$, $M_{DON,RLO}$, and $P_{orb,RLO}$ such that at some point in their subsequent evolution they simultaneously satisfy the following requirements:

1: The instantaneous values of P_{orb}, M_{BH}, and q[5], are all within 2-σ of the observed properties listed in Table 1.

2: The instantaneous value of $T_{eff}$is within the range of permitted[6] values listed in Table 1.

3: Like GRS 1915+105, the system is undergoing transient MT. That is, we require that the rate of accretion onto the BH is less than the critical rate separating transient from persistent behavior (Dubus et al. 1999):

$$\dot{M}_{BH} < \dot{M}_{crit} \approx \left(\frac{M_{BH}}{M_\odot}\right)^{\frac{1}{2}} \left(\frac{M_{don}}{M_\odot}\right)^{0.2} \left(\frac{P_{orb}}{1day}\right)^{1.4} \frac{M_\odot}{day} \tag{5}$$

4: The simultaneous satisfaction of requirements 1-3 occurs within the age of the universe (13.7 Gyr)

Although it does not come into play in the case of GRS 1915+105, there is an additional requirement imposed on the Kerr spin parameter a^* of the BH: As matter is accreted onto the BH, angular momentum is transferred from the donor, effectively "spinning up" the BH. Assuming no natal spin on the BH, one can calculate (see equations 9 and 10 in Sørensen et al. (2017)) the accreted spin a^*_{acc} as a function of the total mass accreted by the BH. In the case of non-zero natal spin, a^* will exceed this value. Therefore, observational ranges of a^* function only as an upper limit on

[2] the exception being T_{eff}, as the range of values listed in table 1 cannot be interpreted as having a mean with some associated error. It is therefore only used to rule out potential winners

[3] We will ultimately weight our prior by existing mass and orbital-separation distributions for the galactic population. At the time of writing this step has not been performed. We do, however, draw initial eccentricities from a thermal distribution $f(e) = 2ede$

[4] aside from companion winds, the masses will remain unchanged until RLO

[5] $M_{DON,obs}$is derived from $M_{BH,obs}$and q_{obs}, so the constraints on $M_{BH}$and $q$guarantee the satisfaction of any constraint on M_{DON}

[6] See Table footnote c

a^*_{acc}; any spin not accounted for by a^*_{acc} can be chalked up to non-zero natal spin, but values a^*_{acc} above the maximum observed spin is clearly not compatible with observation. In the case of GRS 1915+105, the spin is extremely high – $a^* > 0.98$ (McClintock et al. 2006) – and the upper limit is simply the maximum possible spin of 1. In future studies of systems with lower spins, this constraint will provide a useful lower limit on $M_{BH,RLO}$

3.1. *Analytic Grid*

FIG. 1.— Potential winning RLO parameters as identified by equation (8a) with $\alpha = 0$, $\beta = 0$. Note how at low values of $M_{BH,RLO}$, only shorter periods are viable. The amount of mass that would need to be accreted to satisfy the constraint on M_{BH} would lengthen the period well past $P_{orb,obs}$ for all but the shortest RLO periods.

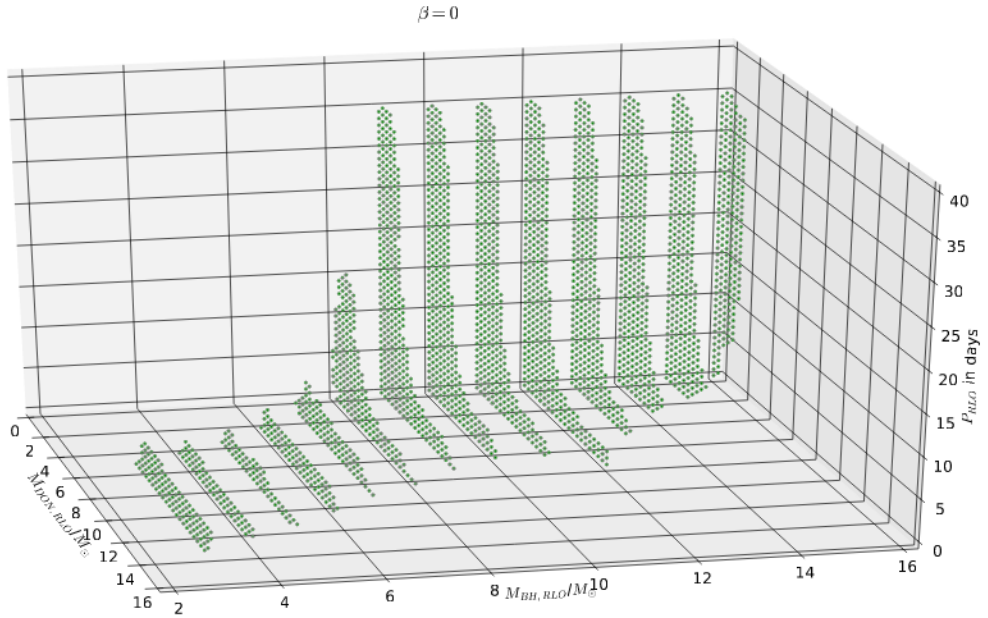

Detailed MESA calculations are computationally expensive, so we first narrow down the parameter-space analytically.

We follow the approach of Sørensen et al. (2017) and begin by assuming a simple point mass model in a circular orbit, ignoring stellar structure and focusing on orbital changes due to angular momentum transfer from the donor to the accretor through the first Lagrangian point. In what follows, M_{DON} and M_{BH} are the instantaneous donor and black hole masses, a is the instantaneous orbital separation, α is the fraction of mass lost from the donor, and β is the fraction of mass lost from the vicinity of the accretor, after the mass has been funneled through the Lagrangian point L1 at an efficiency of $1 - \alpha$. We begin by solving equation 6[7] in Sørensen et al. (2017), derived from appeal to conservation of angular momentum.

$$\frac{da}{dM_{DON}} = \frac{2a}{M_{DON}}\left(\alpha(1-q) - (1-a) + \frac{q}{2(1+q)}(\alpha\beta - \alpha - \beta)\right) \tag{6}$$

Plugging in $q = \frac{M_{DON}}{M_{BH}}$ and rearranging, we have

$$\frac{da}{2a} = dM_{DON}\left(\frac{\alpha - 1}{M_{DON}} + \frac{1-\alpha}{M_{BH}} + \frac{\alpha\beta - \alpha - \beta}{2(M_{BH} + M_{DON})}\right) \tag{7}$$

At the same time, $\dot{M}_{BH} = -(1-\alpha)(1-\beta)\dot{M}_{DON}$. Writing $(1-\alpha)(1-\beta) = C$ Integrating both sides with respect to time gives

$$M_{BH} - M_{BH_RLO} = -C(M_{DON} - M_{DON,RLO}) \tag{8}$$

[7] When I was working on this problem, the Sørensen et al. (2017) paper was a rough draft that only mentioned numerically solving equation 6. Since then, they've included an analytic solution. I'm leaving this here anyway because it is representative of my early work on this project.

FIG. 2.— Potential winning RLO parameters as identified by equation (8a) with $\alpha = 0$, $\beta = 1$. Since no matter will actually accrete onto the BH, the only viable values of $M_{BH,RLO}$ are those that already satisfy the observational constraint on MBH

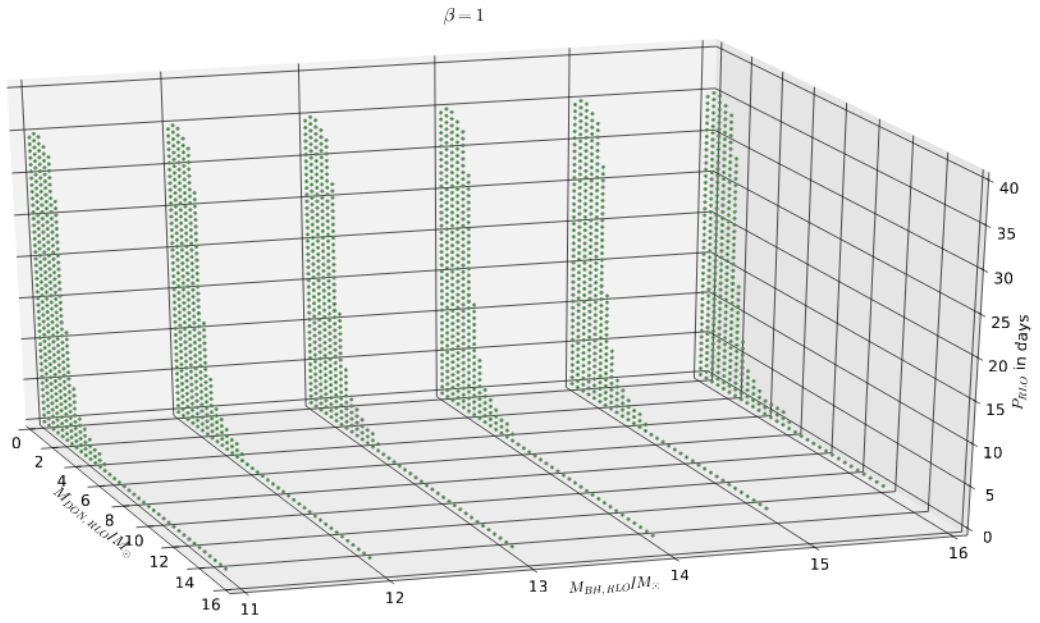

where $M_{BH,RLO}$ and $M_{DON,RLO}$ are just the masses of the BH and donor at the onset of mass transfer ($M_{BH,RLO}$ and $M_{DON,RLO}$). Using this to rewrite M_{BH} in the rearranged equation and recognizing that we've successfully separated our variables allows us to write

$$\int \frac{da}{2a} = \int \frac{\alpha - 1}{M_{DON}} dM_{DON} + \int \frac{1-\alpha}{-CM_{DON} + CM_{DON,RLO} + M_{BH,RLO}} dM_{DON} + \int \frac{\alpha\beta - \alpha - \beta}{2((1-C)M_{DON} + CM_{DON,RLO} + M_{BH,RLO}} \tag{9}$$

If either α or β is 1, then $C = 0$ and

$$\frac{1}{2}\ln\left(\frac{a}{a_{RLO}}\right) = (\alpha-1)\ln\left(\frac{M_{DON}}{M_{DON,RLO}}\right) + (1-\alpha)\left(\frac{M_{DON} - M_{DON,RLO}}{M_{BH,RLO}}\right) + \frac{(\alpha\beta - \alpha - \beta)}{2}\ln\left(\frac{M_{DON} + M_{BH,RLO}}{M_{DON,RLO} + M_{BH,RLO}}\right) \tag{10}$$

Otherwise, $C \neq 0$ and

$$\begin{aligned}\frac{1}{2}\ln\left(\frac{a}{a_{RLO}}\right) = (\alpha-1)\ln\left(\frac{M_{DON}}{M_{DON,RLO}}\right) + (\beta-1)\ln\left(\frac{M_{BH,RLO} + C(M_{DON,RLO} - M_{DON})}{M_{BH,RLO}}\right) \\ + \frac{\alpha\beta - \alpha - \beta}{2(1-C)}\ln\left(\frac{(1-C)M_{DON} + M_{DON,RLO} + M_{BH,RLO}}{M_{DON,RLO} + M_{BH,RLO}}\right)\end{aligned} \tag{11}$$

Expanding C, writing a and a_{RLO} in terms of P and P_{RLO}, M_{DON} as qM_{BH}, exponentiating both sides and cleaning up, we get

$$P = P_{RLO}\left(\frac{qM_{BH}}{M_{DON,RLO}}\right)^{3(\alpha-1)}\left(\frac{M_{DON,RLO} + M_{BH,RLO}}{(1+q)M_{BH}}\right)^2 e^{(1-\alpha)(q - \frac{M_{DON,RLO}}{M_{BH}})}, \qquad \alpha \text{ or } \beta \ = 1 \tag{12a}$$

$$P = P_{RLO}\left(\frac{qM_{BH}}{M_{DON,RLO}}\right)^{3(\alpha-1)}\left(\frac{M_{DON,RLO} + M_{BH,RLO}}{(1+q)M_{BH}}\right)^2\left(\frac{M_{BH,RLO}}{M_{BH}}\right)^{\frac{3}{\beta-1}}, \quad \alpha < 0 \text{ and } \beta < 0 \tag{12b}$$

With equations (12a) and (12b) in hand, we can set α and β and easily check whether a given PPRLO with parameters $M_{BH,RLO}$, $M_{DON,RLO}$, $P_{orb,RLO}$will satisfy requirement 1 by scanning through $M_{BH} \in [M_{BH,obs} -$

FIG. 3.— MESA Results for fully conservative Mass Transfer ($\beta = 0$). The gray points are systems that passed the anaalytic check but ultimately failed to simultaneously satisfy all observational constraints. The constraint on T_{eff} rules out most of these systems. Green points simultaneously satisfied all observational constraints within the age of the universe.

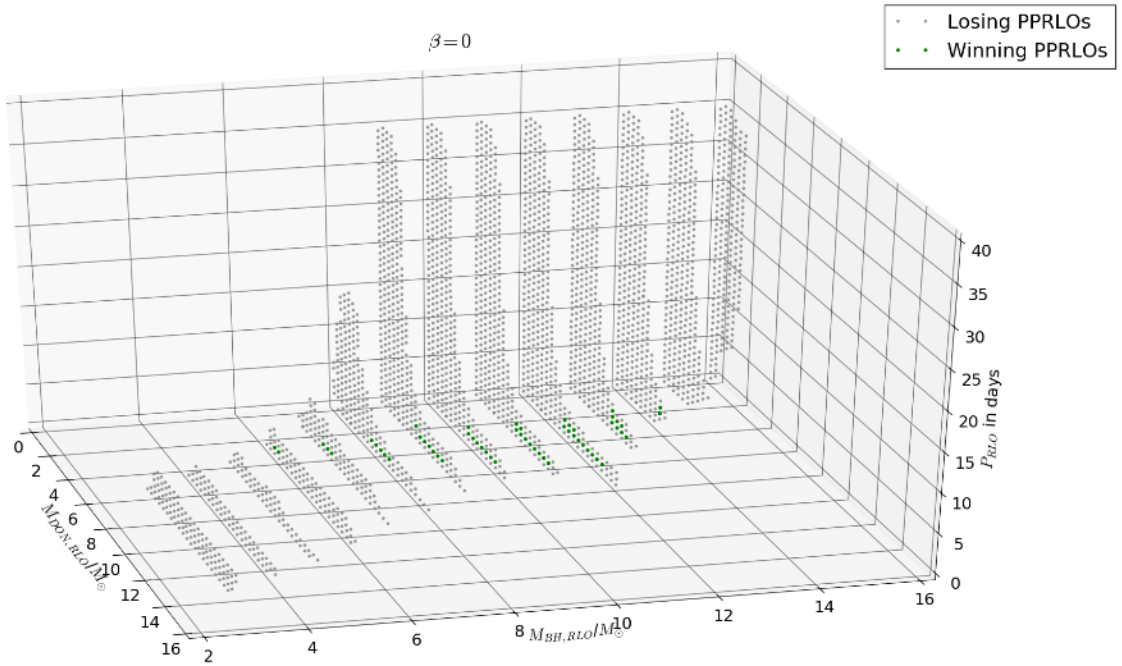

$2\sigma_{Mbh}, M_{BH,obs} + 2\sigma_{Mbh}]$ and $q \in [q_{obs} - 2\sigma_q, q_{obs} + 2\sigma_q]$ to see if $P(M_{BH}, q) \in [P_{obs} - 2\sigma_P, P_{obs} + 2\sigma_P]$. We draw candidate combinations of $M_{BH,RLO}$, $M_{DON,RLO}$, and $P_{orb,RLO}$from a grid bound as follows: $M_{BH,RLO}$is bound from above by the 2-σ upper bound on $M_{BH,obs}$(16.4 $M_\odot$) as, aside from evaporation processes neglected here, it will accrete matter but never lose it. It is bound from below by the Tolman-Oppenheimer-Volkoff limit of around 3.0 $M_\odot$, as we expect supernova remnants below this limit to form neutron stars rather than black holes (Oppenheimer et al. 1939). $M_{DON,RLO}$is bound from above by the 2-σ upper bound on the total mass of the system less the minimum possible 3 $M_\odot$ of its black hole companion (around 16 $M_\odot$. Since this process is computationally cheap, we let $P_{orb,RLO}$vary from 0 to a few years to find the maximum allowable value by brute force. See figures 1 and 2 for the results of our analytic check in the $\beta = 0$ and $\beta = 1$ cases respectively.

3.2. *MESA Sequences*

With our *RLO* parameter space narrowed down analytically by requirement 1 to the grids in figures 1 and 2, it is now feasible to perform detailed stellar structure and binary evolution calculations on all PPRLOs to check against requirements 2-4.

We pass our analytic grid through MESA (Modules for Experiments in Stellar Astrophysics), a publicly available, 1-D stellar evolution code (see Paxton et al. (2015) for the latest instrument paper). We assume solar metallicity for the donor, and activate magnetic breaking once a donor drops below 1.5 $M_\odot$. Our input grid has $M_{BH,RLO}$spaced by 1 $M_\odot$, $M_{DON,RLO}$spaced by 0.4 $M_\odot$, and $P_{orb,RLO}$spaced by 0.8 days. We assume that mass transfer through L1 is perfectly efficient ($\alpha = 0$), and explore the cases of perfectly conservative mass transfer from L1 onto the accretor (β=0), as well as perfectly non-conservative mass transfer from L1 onto the donor (β=1). For each system on our grid, we want RLO to occur *just* as it attains orbital parameters $M_{BH,RLO}$, $M_{DON,RLO}$, and $P_{orb,RLO}$. To ensure this we begin by freezing the orbital parameters and evolving the donor until the moment that it first fills its roche lobe. We then allow the orbit to evolve freely from that point forward.

In figures 3 and 4, we present the results of our MESA simulations. The systems that passed our analytic checks but failed to simultaneously satisfy requirements 1-4 are shown in grey. Those systems that did indeed simultaneously satisfy requirements 1-4 (so-called "winners") are overlaid in green. Unfortunately, the number of winning systems in the $\beta = 1$ case was too low for us to conduct the analysis presented in this paper. We plan on scaling up our simulations to achieve the sort of numbers desired but for now we emphasize that **in all subsequent sections, we restrict ourselves to the $\beta = 0$ case.**

FIG. 4.— MESA Results for fully non-conservative Mass Transfer ($\beta = 1$). As above, gray points are systems that passed the analytic check but ultimately failed to simultaneously satisfy all observational constraints. Green points simultaneously satisfied all observational constraints within the age of the universe. Normally we would seek to "cap off" winners on the borders of our grid in order to make sure we're not missing any. In this case, that would mean running systems with $M_{BH,RLO} = 17$, which is already above the 2-σ range for $M_{BH,obs}$. Since we know the BH in our models will never lose mass, running these systems would be superfluous.

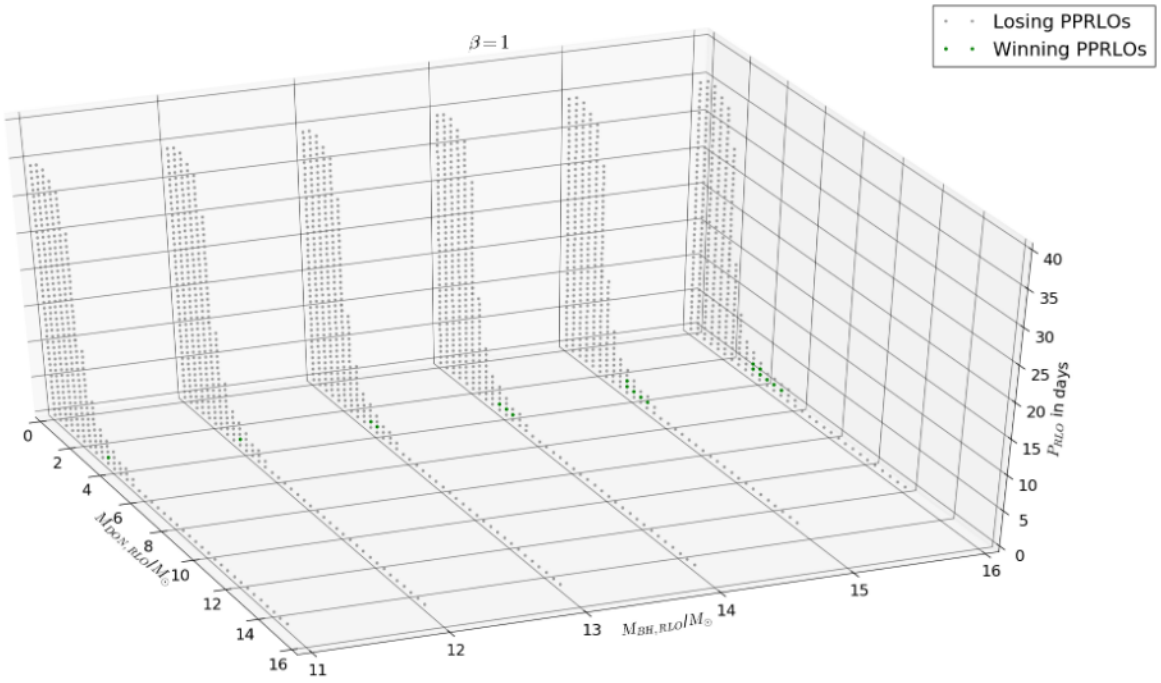

In figures 5 and 6, we present evolutionary tracks for a sample winning system and a sample losing system respectively. Not shown in those plots is the satisfaction of the requirement 3. As it turns out, all systems that satisfied requirements 1,2, and 4 were also transient and satisfied requirement 3.

4. KINEMATIC HISTORY OF GRS 1915+105

In this section we trace the trajectory of GRS 1915+105 through the galactic potential back through time to find possible BH progenitor birth locations. We assume that pre-SN, the progenitor to GRS 1915+105 traveled with the rest of the galactic disk at the average rate of galactic rotation (here, as in Miller-Jones (2014), we adopt a flat galactic rotation curve of a constant 238,000 km/s), and that it was kicked from the galactic plane upon SN. As in Willems et al. (2005), we take the current age of the donor from winning mass transfer sequences as estimates of the time of BH birth, with an uncertainty on the order of the lifetime of the BH progenitor before core-collapse (10 Myrs). We then sample the system's peculiar velocity at crossings of the galactic plane that occur within 10 Myrs of one of these donor ages, giving us a distribution of possible peculiar velocities just after SN. We then use a fit to weight possible progenitor systems by where their peculiar velocity, as outputted by the SN calculations in section 7, falls within this distribution.

We start by fixing a right-handed Cartesian coordinate system XYZ with its origin at the galactic center. We take the X-Y plane to coincide with the galactic plane, with the X axis connecting the sun's projection onto the galactic plane with the galactic center, and the Y axis pointing in the direction of galactic rotation at the location of the sun. The Z axis points toward the galactic north pole, perpendicular to the plane of the galaxy. In this coordinate system, the parameters in 1 ($l = 45.37°, b = -0.22°, and d = 11$ +/-1kpc) coincide with $X = -0.5724$ +/- 0.702kpc, $Y = 7.828$ +/- 0.712kpc, and $Z = -0.40$ +/- 0.006kpc. We take the velocity components compiled in Miller-Jones (2014) of $U = 272$ +/- 23km/s,$V = -230$ +/- 23km/s, and $W = -11$ +/- 4km/s, with U,V,W corresponding to the positive X,Y,and Z directions respectively.

We use the potential from Carlberg & Innanen (1987) with updated parameters from Kuijken & Gilmore (1989). This potential is split into three components

$$\phi_g(r, z) = \phi_{nucleus}(r, z) + \phi_{bulge}(r, z) + \phi_{disk}(r, z) \tag{13}$$

FIG. 5.— An example of a winning mass transfer sequence. The yellow dot indicates the onset of RLO. As noted in section 2.2, we begin with a Zero-Age Main-Sequence donor in an orbit with the desired RLO period and secularly evolve the donor until it fills its Roche Lobe, at which point we allow the orbital parameters to evolve. In the top left and right plots, the red bars mark the 1 and 2-σ ranges on $M_{BH,obs}$ and q_{obs} respectively. In the bottom left plot, the red bars indicate the permitted range of T_{eff} corresponding to the observed spectral types. In the bottom right plot, the green line indicates P_{obs}, and the dashed vertical line in all plots marks the moment the system reaches this observed period. Notice that all tracks cross the dashed line within 2-σ (or just within the permitted range in the case of T_{eff}) of their respective observed quantity, making this system a winning mass transfer sequence.

$M_{BH,RLO} = 11.0 M_\odot$, $M_{DON,RLO} = 6.1 M_\odot$, $P_{RLO} = 0.9 days$

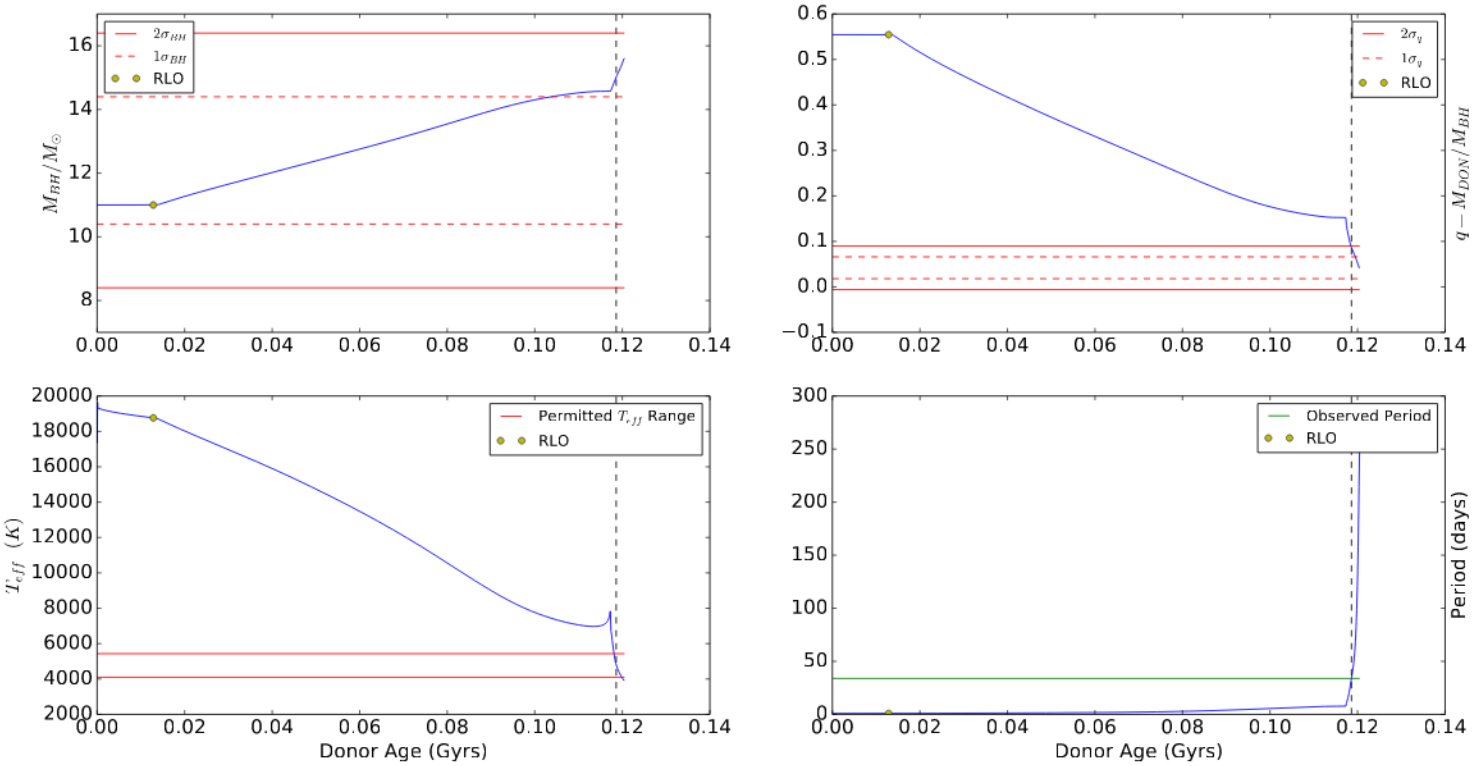

TABLE 2
CONSTANT TERMS IN MODEL OF GALACTIC POTENTIAL

Parameter	Value	Unit
M_{disk}	$1.45x10^{11}$	M_{sun}
M_{bulge}	$9.3x10^{9}$	M_{sun}
$M_{nucleus}$	$1x10^{10}$	M_{sun}
b_{disk}	5.5	kpc
b_{bulge}	0.25	kpc
$b_{nucleus}$	1.5	kpc
h_1	0.325	kpc
h_2	0.090	kpc
h_3	0.125	kpc
a_G	2.4	kpc
β_1	0.4	
β_2	0.5	
β_3	0.1	

All values due to Kuijken & Gilmore (1989)

accounting for mass densities in the the disk halo, bulge, and nucleus respectively. The disk halo term is given by

$$\phi_{disk}(r,z) = \frac{-GM_{disk}}{\sqrt{(a_G + \sum_{i=1}^{3} \beta_i \sqrt{z^2 + h_i^2})^2 + b_{disk}^2 + r^2}} \quad (14)$$

FIG. 6.— An example of a losing mass transfer sequence. The markings are as in figure 5. The donor's effective temperature drops outside of the permitted range just as the system reaches the observed period. Notice how, compared to figure 5, the larger period means that it takes much longer for the donor to fill its Roche Lobe. This is compounded by the smaller mass and hence slower evolution of the donor.

$$M_{BH,RLO} = 8.0 M_\odot,\ M_{DON,RLO} = 1.3 M_\odot,\ P_{RLO} = 2.5 days$$

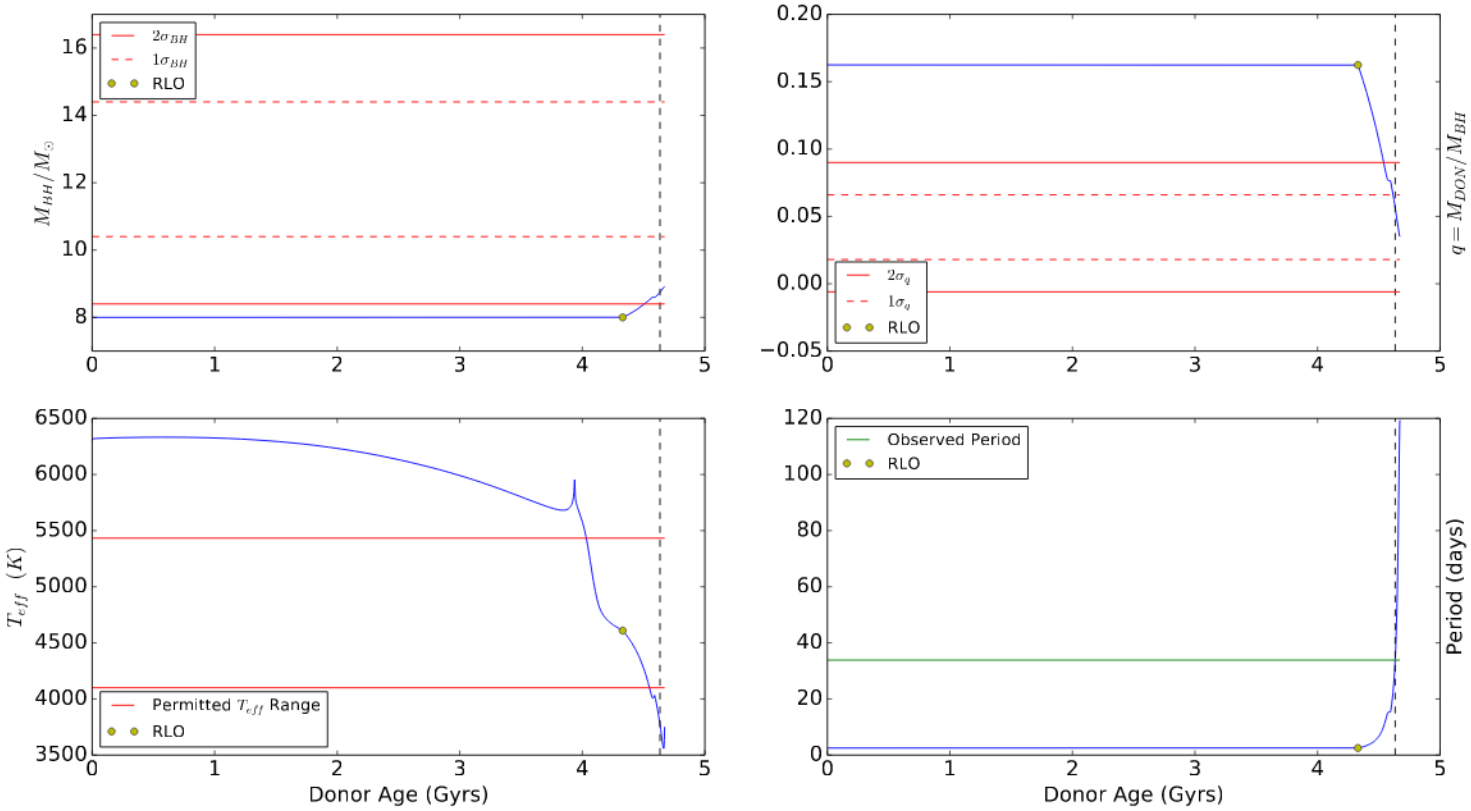

FIG. 7.— Trajectory of GRS 1915+105 through the Galactic Potential over the past 5 Gyrs. The blue track corresponds to initial conditions equal to the central observational values, while the gray tracks correspond to random combinations of initial conditions within 1-σ of the observational values. The red dot indicates the current location of GRS 1915+105.

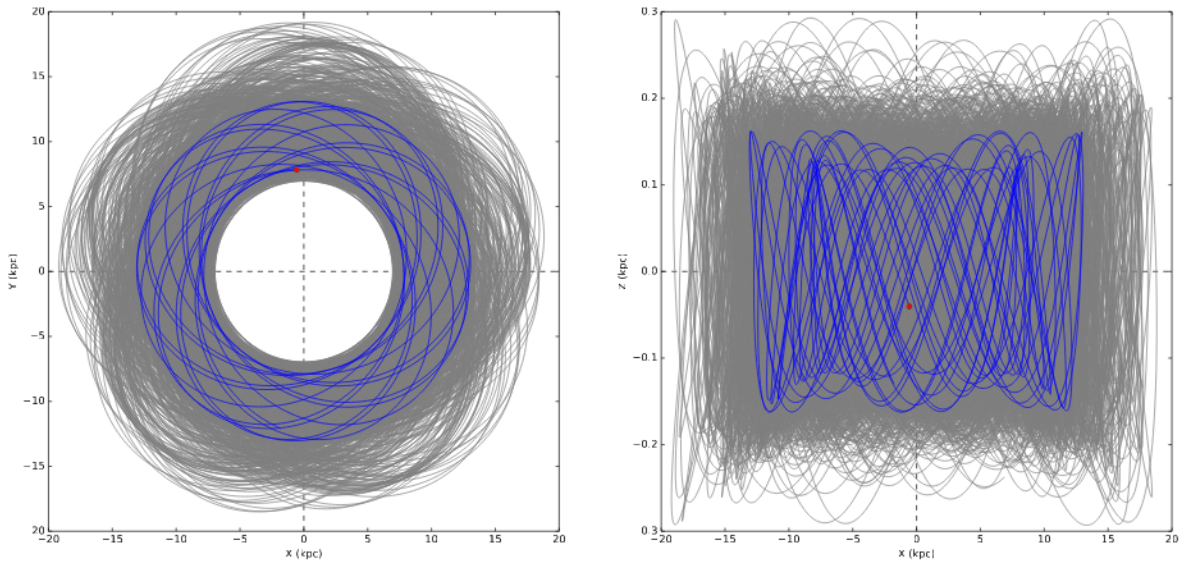

FIG. 8.— Peculiar Velocity of GRS 1915+105 through the Galactic Potential. The peculiar velocity is obtained by subtracting the galactic rotation from the space-velocity of the system. We use a flat 238,000 km/s as our galactic rotation curve. The blue track corresponds to initial conditions equal to the central observational values, while the gray tracks correspond to random combinations of initial conditions within 1-σ of the observational values.

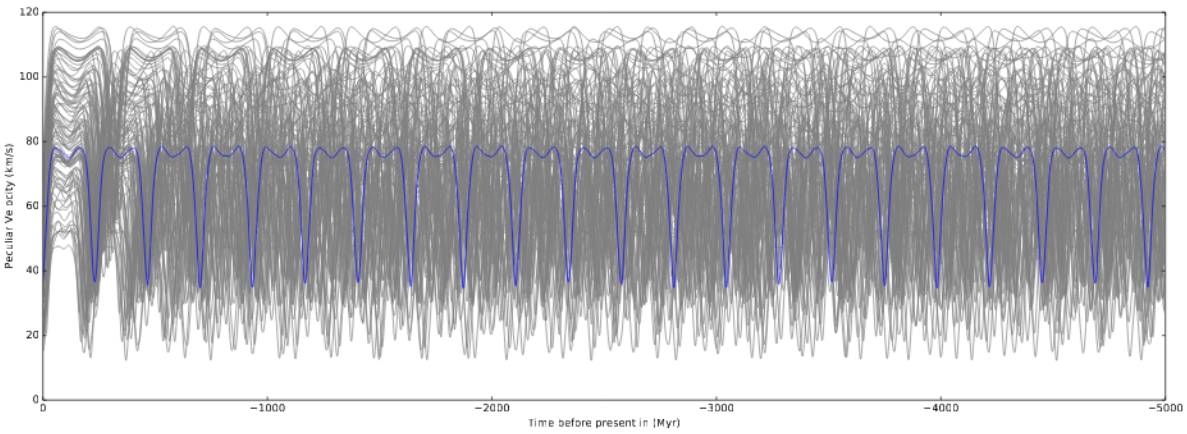

FIG. 9.— Histogram of Peculiar Velocities at Crossings of the Galactic Plane within 10 Myrs of potential BH birth times, as estimated from the current donor ages of our winning mass transfer sequences.

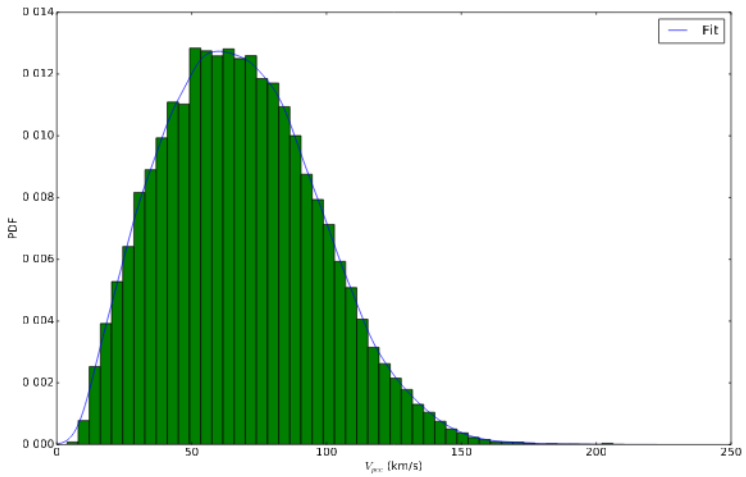

and the bulge and nucleus terms are given by

$$\phi_{bulge}(r) = \frac{-GM_{bulge}}{\sqrt{b_{bulge}^2 + r^2}}, \quad \phi_{nucleus}(r) = \frac{-GM_{nucleus}}{\sqrt{b_{nucleus}^2 + r^2}} \tag{15}$$

We list all constants in Table 2.

In figure 7, we present the trajectory of GRS 1915+105 through the galactic potential over the last 5 Gyrs. In order to obtain the V_{pec} distribution described above and seen in figure 9, we integrated 10,000 trajectories with initial conditions sampled from normal distributions centered on their mean observational values. We see in the right hand panel of figure 7 that, even allowing for these uncertainties, GRS 1915+105 remains within 0.3 kpc of the galactic disk. Meanwhile, we see in figure 8 that the system maintains a peculiar velocity between 18 and 120 km/s at all times.

5. TIDAL EVOLUTION

As the binary evolves post-SN, its orbit changes due to tidal interactions between the donor and BH, angular momentum loss due to stellar winds on the donor, and angular momentum loss due to gravitational radiation. We use single-star MESA simulations of the donor to keep track of wind mass-loss and stellar structure. The evolution of the semi-major axis A, eccentricity e, and the donor's rotational angular velocity Ω are governed by the following

equations derived in Hut et al. (1981)

$$\left(\frac{dA}{dt}\right)_{tides} = -6\frac{k_2}{T}\frac{M_{BH}(M_{BH}+M_{DON})}{M_{DON}^2}\left(\frac{R_{DON}}{A}\right)^8 \frac{A}{(1-e^2)^{15/2}}\left(f_1 - (1-e^2)^{3/2}f_2\frac{\Omega}{n}\right) \tag{16}$$

$$\left(\frac{de}{dt}\right)_{tides} = -27\frac{k_2}{T}\frac{M_{BH}(M_{BH}+M_{DON})}{M_{DON}^2}\left(\frac{R_{DON}}{A}\right)^8 \frac{e}{(1-e^2)^{13/2}}\left(f_3 - \frac{11}{8}(1-e^2)^{3/2}f_4\frac{\Omega}{n}\right) \tag{17}$$

$$\left(\frac{d\Omega}{dt}\right)_{tides} = 3\frac{k_2}{T}\left(\frac{M_{BH}}{M_{DON}}\right)^2 \frac{M_{DON}R_{DON}^2}{I_{DON}}\left(\frac{R_{DON}}{A}\right)^6 \frac{n}{(1-e^2)^6}\left(f_2 - (1-e^2)^{3/2}f_5\frac{\Omega}{n}\right) \tag{18}$$

where f_1, f_2, f_3, f_4, and f_5 are given by

$$f_1 = 1 + \frac{31}{2}e^2 + \frac{255}{8}e^4 + \frac{185}{16}e^6 + \frac{25}{64}e^8 \tag{19}$$

$$f_2 = 1 + \frac{15}{2}e^2 + \frac{45}{8}e^4 + \frac{5}{16}e^6 \tag{20}$$

$$f_3 = 1 + \frac{15}{4}e^2 + \frac{15}{8}e^4 + \frac{5}{64}e^6 \tag{21}$$

$$f_4 = 1 + \frac{3}{2}e^2 + \frac{1}{8}e^4 \tag{22}$$

$$f_5 = 1 + 3e^2 + \frac{3}{8}e^4 \tag{23}$$

and where R_{DON} and I_{DON} are the donor radius and moment of inertia, respectively, n is the average orbital angular velocity, $k2$ is the apsidal-motion constant, and T is a characteristic time-scale for tidal effects on orbital evolution. For the time being, we consider the case of complete synchronization $\left(\frac{\Omega}{n} = 1\right)$ between the rotational and orbital angular velocities, but plan on scanning this parameter in the future to confirm that it does not severely affect our results. We use the approximation for $\frac{k_2}{T}$ given in Willems et al. (2005) and Hurley et al. (2002):

$$\left(\frac{k_2}{T}\right) \approx 1.9782 \text{ x } 10^4 \frac{R_{DON}}{R_\odot}\left(\frac{M_{DON}}{M_\odot}\right)^{1/2}\left(\frac{R_\odot}{A}\right)^{5/2}\left(\frac{M_{BH}+M_{DON}}{M_{DON}}\right)^{5/6} E_2 \; yr^{-1} \tag{24}$$

where

$$E_2 = 1.592 \text{ x } 10^{-9}\left(\frac{M_{DON}}{M_\odot}\right)^{2.84} \tag{25}$$

In addition to tidal effects, gravitational radiation will carry away angular momentum, further shrinking and circularizing the orbit. We use the 3.5 post-Newtonian order equations derived by Junker and Schäfer (1992). For brevity, we list the equations only to the lowest order in $\frac{G(M_{BH}+M_{DON})}{Ac^2}$:

$$\left(\frac{dA}{dt}\right)_{GR} = -\frac{M_{BH}M_{DON}}{(M_{BH}+M_{DON})^2}\frac{2c}{15(1-e^2)^{7/2}}\left(\frac{G(M_{BH}+M_{DON})}{Ac^2}\right)^3 (96 + 292e^2 + 37e^4) \tag{26}$$

$$\left(\frac{de}{dt}\right)_{GR} = -\frac{M_{BH}M_{DON}}{(M_{BH}+M_{DON})^2}\frac{c^3}{15G(M_{BH}+M_{DON})}\left(\frac{G(M_{BH}+M_{DON})}{Ac^2}\right)^4 \frac{e(304+121e^2)}{(1-e^2)^{5/2}} \tag{27}$$

where c is the speed of light.

As input to our calculations, we sample every winning combination of $M_{BH,RLO}$, $M_{DON,RLO}$from our MESA simulations, and for each such combination we scan a grid of A_{postSN}, e_{postSN}, where A_{postSN} ranges in increments of 1 $R_\odot$from 0 to 1200 $R_\odot$non-inclusive, and e_{postSN} ranges from 0 to 1 in increments of 0.05. We use the stiff LSODE numerical solver included in the odespy[8] numerical package to evolve each system until the donor fills its roche lobe, at which point match the output of our SN calculations to the grid that we fed into the tidal evolution calculations, and then we match each of our tidally evolve systems to a unique winning MT sequence. The matching conditions are described below.

[8] H. P. Langtangen and L. Wang. Odespy software package. URL: https://github.com/hplgit/odespy. 2015

6. ZAMS TO CORE-COLLAPSE

Identifying possible progenitor systems of GRS 1915+105 provides a broad constraint on its historical parameters, but in order assess the likelihood of one PPS over another we must find a way to evaluate their relative formation rates. In an attempt to do just this, we use the computationally cheap and publicly available parametric Binary Stellar Evolution software BSE (Hurley et al. 2002) to evolve an initial population of 1,000,000 stellar binaries with ZAMS components to obtain a reasonably sized population of viable pre-SN progenitor systems. We start with 1,000,000 primary masses between 0 and 100 $M_{\odot}$(the maximum initial mass allowed by BSE), drawn from a flat distribution, with secondary masses obtained from drawing a mass ratio q from a flat distribution between 0 and 1. Orbital semi-major axes are drawn from a logarithmic distribution between 0 and 100,000 $R_{\odot}$, and orbital eccentricities are drawn from a thermal distribution $f(e) = 2ede$ between 0 and 1. To avoid making model-specific assumptions of SN dynamics, we stop each simulation just before the core-collapse of the primary, feeding the pre-SN parameters into the SN calculations described in the next section. In figure 10 we present scatter-plots of the ZAMS and pre-SN system parameters, highlighting those systems that eventually match a winning PPRLO.

FIG. 10.— Scatter-plots of ZAMS and pre-SN parameters from our BSE simulations. We highlight those systems that go on to match a winning mass transfer sequence. In the lower right-hand plot one can see that, as expected, all viable PPS have circularized before SN, having gone through a common-envelope phase that shed the hydrogen-rich envelope of the primary, leaving a helium core pre-collapse.

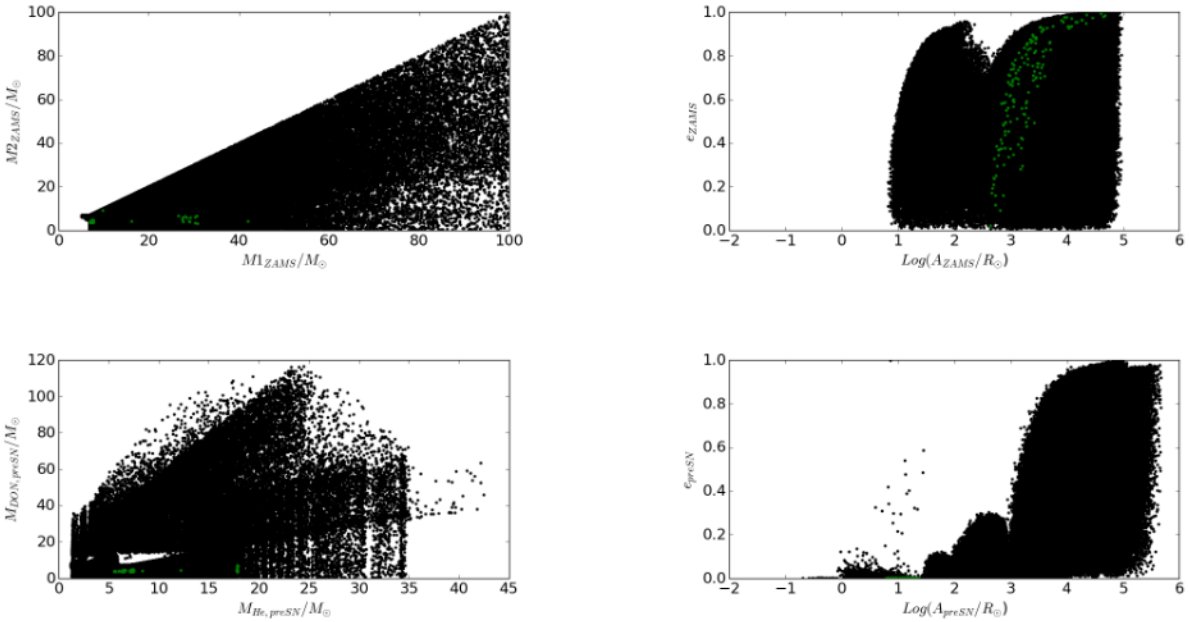

[ht]

7. SUPERNOVA CALCULATIONS

For each system that survived the BSE simulations up to core collapse, we have a set of parameters $M_{He,preSN}, M_{DON}, A_{preSN}, e_{pr}$ describing the mass of the helium-core BH progenitor, the mass of the eventual donor companion, and the orbital semi-major axis and eccentricity just before core-collapse and SN. During the SN, the system will lose some mass $M_{loss} = M_{He,preSN} - M_{BH,postSN}$ and receive a kick V_{kick} that will change its orbital parameters. For each pre-SN system, we randomly sample 1000 values of post-SN black hole mass $M_{BH,postSN}$ uniformly from a minimum of 3 $M_{\odot}$to a maximum of the progenitor mass $M_{He,preSN}$, kick magnitude V_{kick} from $0 - 1000km/sec$, kick direction θ, ϕ, and pre-SN mean anomaly m. Here θ is the polar angle between the relative orbital velocity of the helium-core BH progenitor and the kick velocity, and ϕ is the azimuthal angle defined such that $\phi = 0$ is the plane perpendicular to the line connecting the two masses. The relationship between pre-SN and post-SN parameters are obtained by appeal to conservation of angular momentum and energy. The original expressions were derived by Hills (1983).
We start by obtaining the eccentric anomaly E_{preSN} from the mean anomaly m by way of the relation

$$m = E_{preSN} - e_{preSN} \cos E_{preSN} \tag{28}$$

solved using the Newton-Raphson method. Then the orbital separation r between the progenitor and donor masses just before SN is given by

$$r = A_{preSN}(1 - e_{preSN} \cos E_{preSN}) \tag{29}$$

FIG. 11.— Scatter-plots of system parameters in the moments just before and after SN. We highlight those systems that eventually go on to match a winning mass transfer sequence.

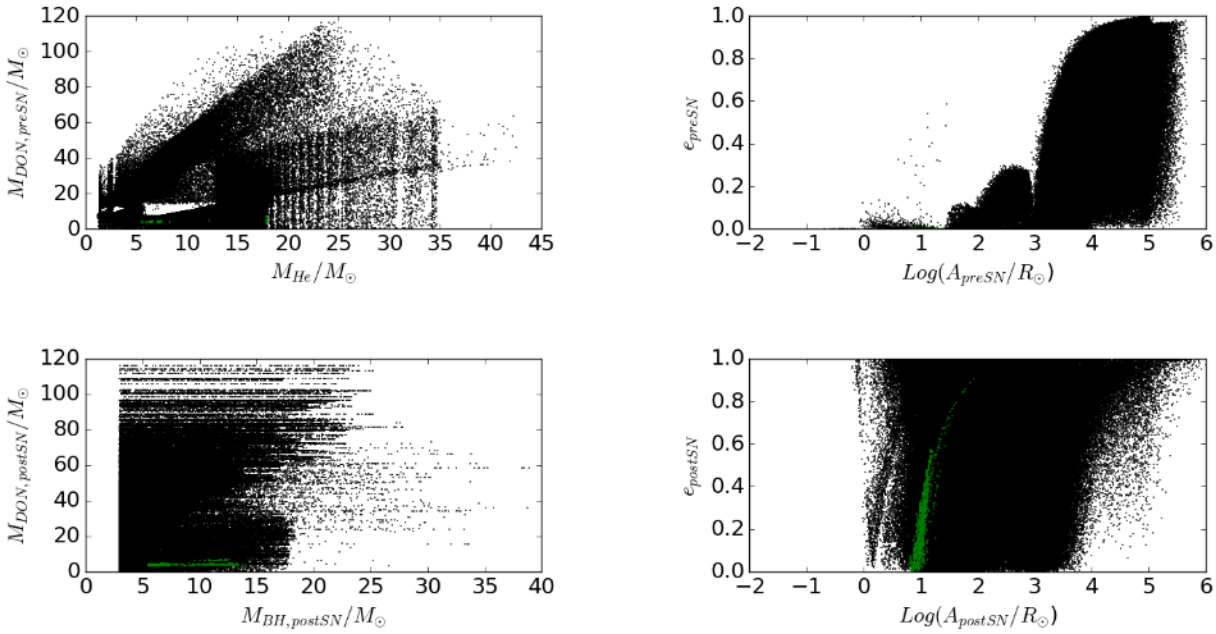

The post-SN semi-major axis is then

$$A_{postSN} = \left(\frac{2}{r} - \frac{V_{He,preSN}^2 + V_{kick}^2 + V_{He,preSN} V_{kick} \cos\theta}{G(M_{BH,postSN} + M_{DON})} \right)^{-1} \tag{30}$$

where G is the newton's gravitational constant and $V_{He,preSN}$ is the pre-SN velocity of the helium-core BH progenitor, given by

$$V_{He,preSN} = \sqrt{G(M_{He,preSN} + M_{DON}) \left(\frac{2}{r} - \frac{1}{A_{preSN}} \right)} \tag{31}$$

Note that since the donor mass is unchanged during the SN, we drop the preSN and postSN subscripts when referring to it for convenience. Next, our post-SN eccentricity is given by

$$e_{postSN} = \sqrt{1 - \frac{r^2 \left(V_{kick}^2 \cos^2\phi \sin^2\theta + (\sin\psi (V_{He,preSN} + V_{kick}\cos\theta) - V_{kick}\cos\psi \sin\theta \sin\phi)^2 \right)}{G A_{postSN} (M_{BH,postSN} + M_{DON})}} \tag{32}$$

where ψ is the angle between the position vector of the progenitor and its pre-SN velocity in the frame of the donor, obtained from

$$\sin\psi = \frac{\sqrt{G(M_{He,preSN} + M_{DON})(1 - e_{preSN}^2) A_{preSN}}}{r V_{He,preSN}} \tag{33}$$

Requiring the binary to remain bound post-SN imposes restrictions on the post-SN parameters. First, continuity requires that the post-SN orbit passes through the pre-SN locations of the donor and progenitor (Flannery et al. 1975), so we must have

$$A_{preSN}(1 - e_{preSN}) \geq A_{postSN}(1 - e_{postSN}) \tag{34}$$

and

$$A_{preSN}(1 + e_{preSN}) \leq A_{postSN}(1 + e_{postSN}) \tag{35}$$

Next, we impose lower and upper limits on the amount of orbital contraction and expansion given the amount of mass lost and the magnitude of the imparted kick, taken from Kalogera & Lorimer (2000)

$$2 - \frac{M_{He,preSN} + M_{DON}}{M_{BH,postSN} + M_{DON}} \left(\frac{V_{kick}}{V_{He,preSN}} + 1 \right)^2 \leq \frac{A_{preSN}}{A_{postSN}} \leq 2 - \frac{M_{He,preSN} + M_{DON}}{M_{BH,postSN} + M_{DON}} \left(\frac{V_{kick}}{V_{He,preSN}} - 1 \right)^2 \tag{36}$$

Finally, we require that the post-SN eccentric anomaly E_{postSN} is real. We use the fact that continuity requires r to be unchanged from the instant before to the instant after SN, so that

$$r = A_{preSN}(1 - e_{preSN}\cos E_{preSN}) = A_{postSN}(1 - e_{postSN}\cos E_{postSN}) \tag{37}$$

and we require that

$$\cos E_{postSN} = \frac{1}{e_{postSN}}\left(1 - \frac{A_{preSN}}{A_{postSN}}(1 - e_{preSN}\cos E_{preSN})\right) \leq 1 \tag{38}$$

If the system satisfies the above restrictions, remaining bound post-SN, we finally calculate the post-SN peculiar velocity of the system's center of mass, imparted by the kick during SN. Using relations derived in Kalogera et al. (1996), we find that

$$V_{pec,postSN} = \sqrt{v_1 V_{He,preSN}^2 + v_2 V_{BH,postSN}^2 + v_3 V_{kick}^2} \tag{39}$$

where $V_{pec,postSN}$ is the relative post-SN orbital velocity of the BH, given by

$$V_{BH,postSN} = \sqrt{G(M_{BH,postSN} + M_{DON})\left(\frac{2}{A_{preSN}} - \frac{1}{A_{postSN}}\right)} \tag{40}$$

and the coefficients v_1, v_2, and v_3 are given by

$$v_1 = \frac{M_{He,preSN}M_{DON}(M_{He,preSN} - M_{BH,postSN})}{(M_{BH,postSN} + M_{DON})(M_{He,preSN} + M_{DON})^2} \tag{41}$$

$$v_2 = -\frac{M_{He,preSN}M_{DON}(M_{He,preSN} - M_{BH,postSN})}{(M_{BH,postSN} + M_{DON})^2(M_{He,preSN} + M_{DON})} \tag{42}$$

$$v_3 = \frac{M_{BH,postSN}M_{He,preSN}}{(M_{BH,postSN} + M_{DON})(M_{He,preSN} + M_{DON})} \tag{43}$$

8. TYING EVOLUTIONARY STAGES TOGETHER

In order to conduct the desired analysis as described in section 2.1, we need to associate each system that is simulated from ZAMS through supernova with a unique system from our simulations of tidal evolution, and then each system from said simulations to a unique winning system from our MESA simulations.

The first task is fairly straightforward. We simply attach a post-SN system to a tidal simulated system if all post-SN parameters (BH and donor masses, semi-major axis, and eccentricity) fall within that tidal system's "cell" on the grid of initial conditions. That is, if the output of our SN calculations is ($M_{BH,postSN}$,$M_{DON,postSN}$,A_{postSN},e_{postSN}) and the input of our tidal calculations is ($M^0_{BH,postSN}$,$M^0_{DON,postSN}$,A^0_{postSN},e^0_{postSN}), we consider the systems a "match" if $M_{BH,postSN} \in (M^0_{BH,postSN} - .5M_\odot, M^0_{BH,postSN} + .5M_\odot)$, $M_{DON,postSN} \in (M^0_{DON,postSN} - 0.2M_\odot, M^0_{DON,postSN} + 0.2M_\odot)$, $A_{postSN} \in (A^0_{postSN} - .5R_\odot, A^0_{postSN} + .5R_\odot)$, and $e_{postSN} \in (e^0_{postSN} - 0.025, e^0_{postSN} + 0.025)$. Finally, we associate each system from our tidal calculations with a unique winning mass transfer sequence. For most combinations of $M_{BH,RLO}$and $M_{DON,RLO}$, there are multiple winning mass transfer sequences, differentiated only by period. To handle this, we match the tidal and MT sequences by angular momentum. That is, if $L_{tidal}(M_{BH,RLO}, M_{DON,RLO}, A_{RLO}, e_{RLO})$ is the angular momentum of a tidally evolved system at the onset of RLO, and $L_{MT}(M_{BH,RLO}, M_{DON,RLO}, P_{orb,RLO})$ is the angular momentum of a winning mass transfer sequence (the input to our MESA simulations), then the two systems are associated with one another if $L_{MT}(M_{BH,RLO}, M_{DON,RLO}, P_{orb,RLO} - dP) < L_{tidal}(M_{BH,RLO}, M_{DON,RLO}, A_{RLO}, e_{RLO}) \leq L_{MT}(M_{BH,RLO}, M_{DON,RLO}, P_{orb,RLO} + dP)$, where $dP = .4days$ is the half-width of the spacing of the periods on the grid used as input to MESA.

9. RESULTS AND DISCUSSION

With all stages of evolution tied together – each BSE through SN simulation associated with a unique tidal simulation, which are in turn associated with unique MESA mass transfer sequences – we now construct probability density functions for all parameters, weighted by the terms in equation 2, allowing us to constrain the properties of GRS 1915+105 at each stage of its evolution. In figures 12 through 15, we present histograms of each parameter, along with weighted Gaussian Kernel Density Estimates (GKDEs). A weighted GKDE is constructed by centering a Gaussian kernel about each data point, scaling it by the desired weight, summing over all of the curves, and then normalizing the entire distribution.

In figure 12 we see PDFs for the ZAMS BH and donor progenitors, and ZAMS semi-major axis and eccentricity. While the donor mass, semi-major axis, and eccentricity are well constrained to single ranges, the BH progenitor mass is split across three distinct, well separated modes. We suspect that these represent three qualitatively different channels of evolution, but have not gotten the chance to investigate further. It is also possible that the gaps between

FIG. 12.— PDFs of system parameters at ZAMS. The grey bars are normalized histograms, and the colored lines are Kernel Density Estimates with weights corresponding to the factors in equation2, with the dashed blue line carrying weights corresponding to the product over the individual weights. In Table 2 we list the $5^{th} - 95^{th}$ percentile ranges for the final, totally weighted (dashed-blue) KDEs. In the case of $M1_{ZAMS}$, we split the mass range into three modes and calculate three different ranges.

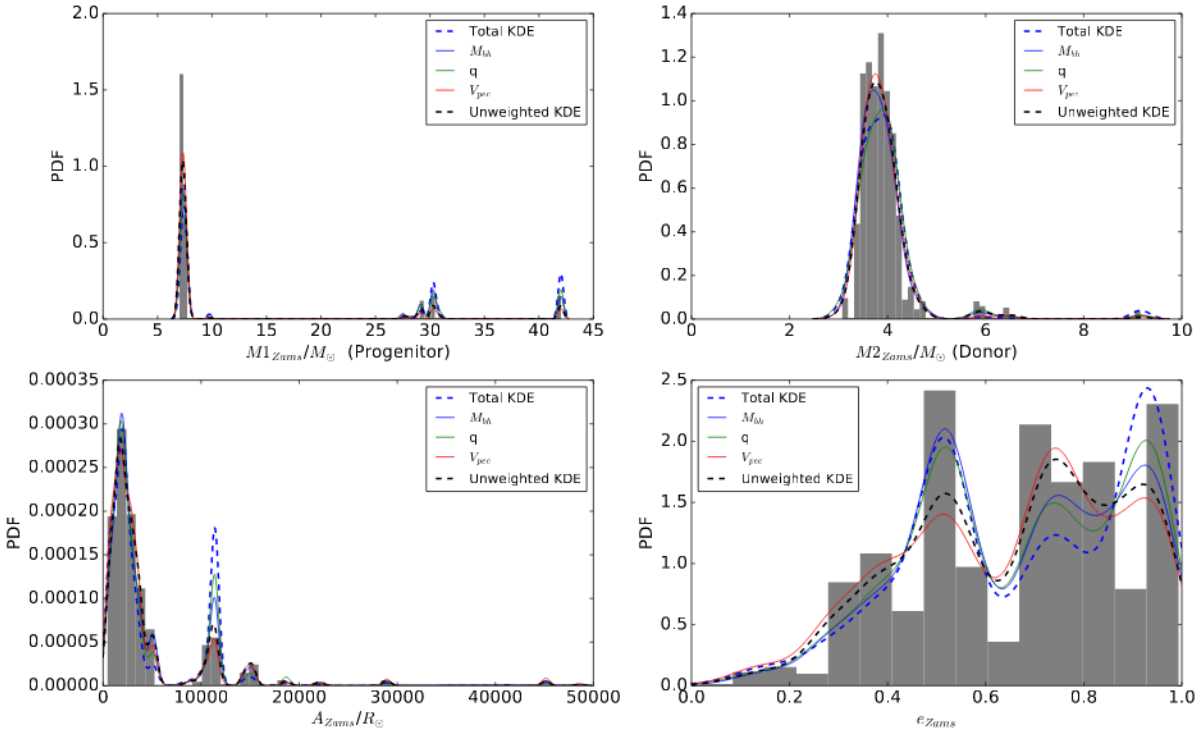

TABLE 3
$5^{th} - 95^{th}$ PERCENTILE RANGES FOR FINAL WEIGHTED PROBABILITY DISTRIBUTIONS.

Parameter	$5^{th} - 95^{th}$ Percentile		
$M1_{ZAMS}$	6.9-8.0	28.0-30.8	41.6-42.4 $M_\odot$
$M1_{ZAMS}$	3.2-4.6 $M_\odot$		
A_{ZAMS}	493.4-11,929.6 $R_\odot$		
e_{ZAMS}	0.29-0.99		
$M_{He,preSN}$	6.3-7.6	12.0-12.4	17.7-18.1 $M_\odot$
A_{preSN}	7.3-16.3 $R_\odot$		
A_{postSN}	8.1-20.0 $R_\odot$		
e_{postSN}	0.04-0.56		
M_{DON} (PreSN,PostSN,RLO)	3.4-4.5 $M_\odot$		
M_{BH} (PostSN,RLO)	3.4-4.5 $M_\odot$		
V_{kick}	11.7-157.2 (km/s)		

modes will eventually populate if we scale up our sample populations and grids. Either way, further investigation is required. For now, treating each mode as a separate distribution, we obtain three ranges representing the 5^{th} to 95^{th} percentiles of each mode, taken from the PDF marked "Total KDE" in figure 12, which carries as weights the product over all of the factors in equation 2. We find that the ZAMS progenitor of the accreting BH in GRS 1915+105 was between either 6.9 and 8.0 $M_\odot$, 28.0 and 30.8 $M_\odot$, or 41.6 and 42.4 $M_\odot$. In the same fashion, we find that the ZAMS donor progenitor was likely between 3.2 and 4.6 $M_\odot$, the ZAMS semi-major axis between 493.4 and 11,929.6 $R_\odot$, and the ZAMs eccentricity between 0.29 and 0.99.

As seen in figure 13, the distinct groupings of the BH progenitor mass evidently persist throughout the binary's early evolution, remaining distinct at the moment just before core-collapse and supernova. Again treating each grouping as a separate distribution, we take the 5^{th} to 95^{th} percentiles to find that GRS 1915+105's BH had a helium core progenitor between either 6.3 and 6.7 $M_\odot$, 12.0 and 12.4 $M_\odot$, or 17.7 and 18.1 $M_\odot$. Meanwhile the donor progenitor, just before the core-collapse of its companion, was likely between 3.4 and 4.5 $M_\odot$, while the semimajor axis was likely

FIG. 13.— PDFs of system parameters just before supernova, as well as the kick velocity imparted at supernova. The grey bars are normalized histograms, and the colored lines are Kernel Density Estimates with coloring as in Fig 8. We omit the e_{preSN} parameter, as it is uniformly within 10^-7 of 0. In Table 2 we list the $5^{th} - 95^{th}$ percentile ranges for the final, totally weighted (dashed-blue) KDEs, with the exception of those corresponding to e_{postSN}. In the case of $M_{He,preSN}$, we split the mass range into three modes and calculate three different ranges.

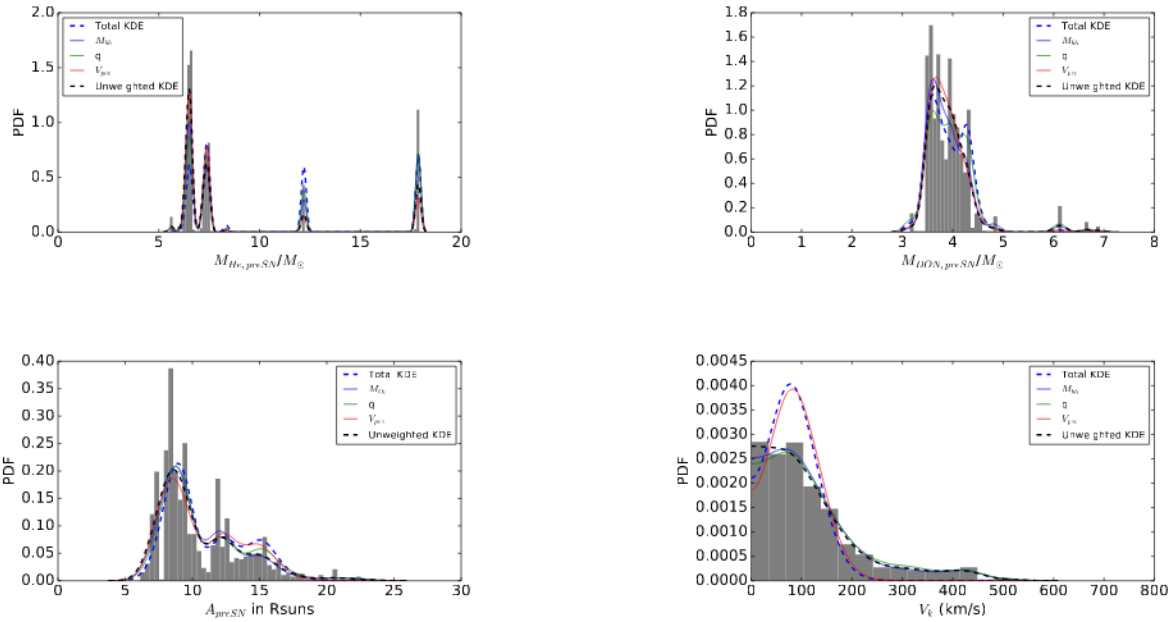

FIG. 14.— PDFs of system parameters just after supernova. The grey bars are normalized histograms, and the colored lines are Kernel Density Estimates with coloring as in Fig 9. In Table 2 we list the $5^{th} - 95^{th}$ percentile ranges for the final, totally weighted (dashed-blue) KDEs.

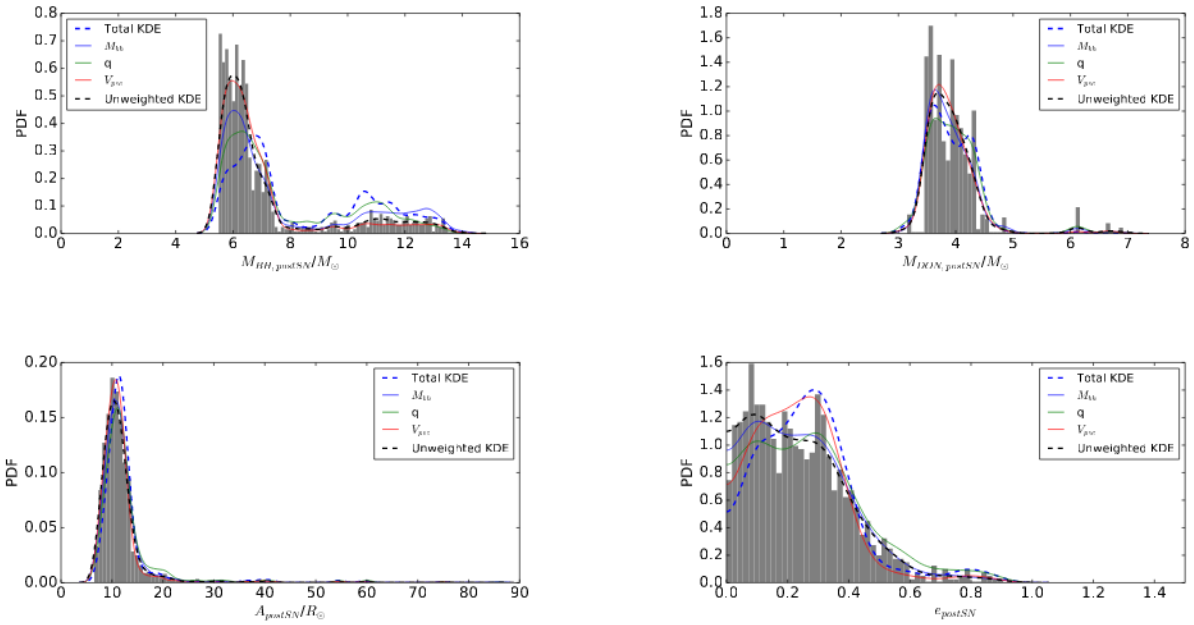

FIG. 15.— PDFs of system parameters just after supernova. The grey bars are normalized histograms, and the colored lines are Kernel Density Estimates with coloring as in Fig 9. We omit the weighted KDEs for P_{RLO}, as data falls on just two points of our grid: P_{RLO}=0.9 and 1.7 days. In Table 2 we list the $5^{th} - 95^{th}$ percentile ranges for the final, totally weighted (dashed-blue) KDEs, with the exception of P_{RLO}.

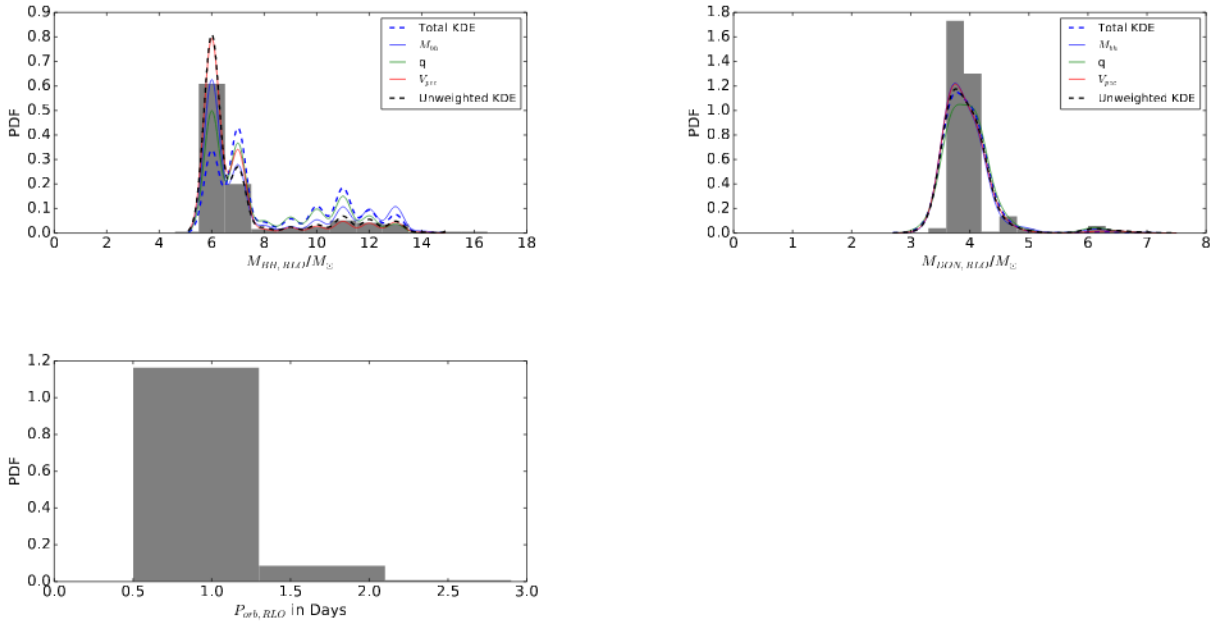

between 7.3 and 16.3 $R_\odot$. We omit PDFs of e_{preSN}, as all values were within 10^-7 of zero. This is as expected, as the common envelope phase rapidly circularizes any eccentric orbits. In the bottom-right panel, we present a histogram and associated pdfs of the magnitude of the kick velocity imparted to the center of mass of the system upon SN. While the kicks were sampled from 0-1000 km/s, it is evident that kicks above 500 km/s were incompatible with a bound post-SN system. It is also notable that the distribution of V_{pec} obtained from our reconstruction of GRS 1915+105's trajectory through the galactic potential is the dominating weight in the total GKDE of V_k. The 5^{th} to 95^{th} percentile range obtained from this pdf suggests that GRS 1915+105 received a kick between 11.7 and 157.2 km/s upon the collapse of the helium core BH progenitor.
In figure 14, we present distributions for the post-SN BH and donor masses, and post-SN semi-major axes and eccentricities. Since our SN calculations assume no mass loss from the donor progenitor, the distribution of post-SN donor masses is obviously identical to that of the pre-SN donor masses. Meanwhile, the BH mass distribution has unified post-SN, with the 5^{th} to 95^{th} suggesting a post-SN BH mass between 5.6 and 12.7 $M_\odot$. Taking the same percentiles for the post-SN semi-major axis and eccentricity yield ranges of 8.1-20.0 and 0.04-5.6 respectively.

Finally, in figure 15, we present distributions for the parameters of GRS 1915+105 at the onset of roche-lobe overflow. Since the mass loss of the BH from post SN to RLO was zero, and that of the donor was negligible, the mass distributions are the same as the post SN masses, with any visual difference owing to the fact that our RLO masses lie on a grid while our post-SN masses are continuously distributed. We omit pdfs of the orbital period at RLO, as we find winning MT sequences for only $P_{RLO} = 0.9$ and 1.7 days. As can be seen in figure 3, this is because those are the only periods that we had any winning MT sequences for, and not because we were unable to produce such systems from our simulations of the ZAMS populations through SN subsequent pre-RLO tidal evolution.

10. CONCLUSION

While our ability to reasonably constrain the properties of GRS 1915+105 at every stage of its evolution is encouraging, we stress that this is an incomplete study. For one, we were only able to obtain these sort of results by assuming fully conservative-mass transfer. Before moving on from GRS 1915+105, we plan to scale up our ZAMS population and tidal and RLO grids for the $\beta = 1$ case in hope of producing winning systems in the sort of numbers that made the above analysis possible. This upscaling will also benefit our analysis of the $\beta = 0$ case, which must also be more closely examined in an attempt to explain the separated BH progenitor mass ranges. We also expect our results to be significantly affected once we incorporate assumptions on the distribution of ZAMS masses and orbital separations in the galactic population.
These contingencies aside, we believe that the work presented here testifies to the viability of our methodology in reconstructing the evolutionary histories of LMXRBs. Upon completion of the GRS 1915+105 analysis, we plan to

repeat this process on V404 Cygni, and possibly on J1655-40 for a modern update of the Willems et al. 2005 study.

REFERENCES

Carlberg, R. G., and K. A. Innanen. 1987. ApJ 94: 66670
Dubus, G., Lasota, J.-P., Hameury, J.-M., & Charles, P. 1999, MNRAS, 303, 139
Dhawan, V., I. F. Mirabel, M. Rib, and I. Rodrigues. 2007, ApJ, 668
Flannery, B. P., & van den Heuvel, E. P. J. 1975, A&A, 39, 61
Fragos, Tassos, and Jeffrey E. McClintock. 2015. ApJ, 800, 17
Gray, David F. 2008. The Observation and Analysis of Stellar Photospheres. 3rd edition. Cambridge: Cambridge University Press
Hills, J. G. 1983. ApJ, 267, 32233
Hurley, Jarrod R., Christopher A. Tout, and Onno R. Pols. 2002. MNRAS, 329, 897928
Hut, P. 1981. A&A 99, 12640
Junker, Wolfgang, and Gerhard Schäfer. 1992. MNRAS, 254, 14664
Kalogera, Vassiliki. 1996. ApJ ,471, 35265
Kalogera, Vassiliki, and Duncan R. Lorimer. 2000, ApJ, 530, 890
Kuijken, Konrad, and Gerard Gilmore. 1989. Monthly Notices of the Royal Astronomical Society 239 (August): 571603
McClintock, Jeffrey E., Rebecca Shafee, Ramesh Narayan, Ronald A. Remillard, Shane W. Davis, and Li-Xin Li. 2006, ApJ, 652, 51839
Miller-Jones, James C. A. 2014, Publications of the Astronomical Society of Australia 31
Oppenheimer, J. R., and G. M. Volkoff. 1939, Physical Review 55, 37481
Paxton, Bill, Pablo Marchant, Josiah Schwab, Evan B. Bauer, Lars Bildsten, Matteo Cantiello, Luc Dessart, et al. 2015, ApJS, 220, 15
Reid, M. J., J. E. McClintock, J. F. Steiner, D. Steeghs, R. A. Remillard, V. Dhawan, and R. Narayan. 2014. ApJ 796
Srensen, Mads, Tassos Fragos, James F. Steiner, Vallia Antoniou, Georges Meynet, and Fani Dosopoulou. 2017, A&A 597, A12
Steeghs, D., J. E. McClintock, S. G. Parsons, M. J. Reid, S. Littlefair, and V. S. Dhillon. 2013. ApJ, 768, 185
Willems, B., M. Henninger, T. Levin, N. Ivanova, V. Kalogera, K. McGhee, F. X. Timmes, and C. L. Fryer. 2005. ApJ, 625, 32446